AGU ADVANCING EARTH AND SPACE SCIENCES

JAMES | Journal of Advances in Modeling Earth Systems®

RESEARCH ARTICLE
10.1029/2023MS004115

Special Collection:
Machine learning application to Earth system modeling

Machine Learning Driven Sensitivity Analysis of E3SM Land Model Parameters for Wetland Methane Emissions

Sandeep Chinta[1], Xiang Gao[1], and Qing Zhu[2]

[1]Center for Global Change Science, Massachusetts Institute of Technology, Cambridge, MA, USA, [2]Climate and Ecosystem Sciences Division, Climate Sciences Department, Lawrence Berkeley National Laboratory, Berkeley, CA, USA

Key Points:

- Identified five key sensitive parameters for methane emissions using the Sobol sensitivity analysis method
- Parameters linked to production and diffusion present the highest sensitivities despite apparent seasonal variation
- Fourteen out of nineteen model parameters exert negligible influence on methane emissions

Supporting Information:

Supporting Information may be found in the online version of this article.

Correspondence to:

S. Chinta,
sandeepc@mit.edu

Citation:

Chinta, S., Gao, X., & Zhu, Q. (2024). Machine learning driven sensitivity analysis of E3SM land model parameters for wetland methane emissions. *Journal of Advances in Modeling Earth Systems*, *16*, e2023MS004115. https://doi.org/10.1029/2023MS004115

Received 13 NOV 2023
Accepted 1 JUL 2024

Author Contributions:

Conceptualization: Sandeep Chinta, Xiang Gao
Data curation: Sandeep Chinta
Formal analysis: Sandeep Chinta, Xiang Gao, Qing Zhu
Investigation: Sandeep Chinta, Xiang Gao, Qing Zhu
Methodology: Sandeep Chinta, Xiang Gao, Qing Zhu
Supervision: Xiang Gao, Qing Zhu
Validation: Sandeep Chinta

Abstract Methane (CH_4) is globally the second most critical greenhouse gas after carbon dioxide, contributing to 16%–25% of the observed atmospheric warming. Wetlands are the primary natural source of methane emissions globally. However, wetland methane emission estimates from biogeochemistry models contain considerable uncertainty. One of the main sources of this uncertainty arises from the numerous uncertain model parameters within various physical, biological, and chemical processes that influence methane production, oxidation, and transport. Sensitivity Analysis (SA) can help identify critical parameters for methane emission and achieve reduced biases and uncertainties in future projections. This study performs SA for 19 selected parameters responsible for critical biogeochemical processes in the methane module of the Energy Exascale Earth System Model (E3SM) land model (ELM). The impact of these parameters on various CH_4 fluxes is examined at 14 FLUXNET- CH_4 sites with diverse vegetation types. Given the extensive number of model simulations needed for global variance-based SA, we employ a machine learning (ML) algorithm to emulate the complex behavior of ELM methane biogeochemistry. We found that parameters linked to CH_4 production and diffusion generally present the highest sensitivities despite apparent seasonal variation. Comparing simulated emissions from perturbed parameter sets against FLUXNET-CH_4 observations revealed that better performances can be achieved at each site compared to the default parameter values. This presents a scope for further improving simulated emissions using parameter calibration with advanced optimization techniques.

Plain Language Summary Methane is a critical greenhouse gas, and wetlands are the largest natural source of it. Accurately predicting methane emissions from wetlands is key to tackling climate change. But these predictions, made through computer models, are seldom spot-on. Why? Because there are many factors in the models that lead to uncertain predictions. A major source of this uncertainty arises from the empirical model parameters. Just as tuning a radio dial ensures clear reception, models need properly adjusted parameters for accurate predictions. A sensitivity analysis was performed to determine which parameters are most crucial for accurate predictions. Instead of running the complex numerical model every time, machine learning was employed to create a faster and simpler version. Using this approach, five parameters were pinpointed as particularly sensitive, significantly impacting the predictions. The comparison of model-predicted methane emissions with real-world measurements showed that the model performed well in some cases but needed tweaking in others. Refining these sensitive parameters with more real-world observations could make better predictions in the future.

1. Introduction

Methane (CH_4) is the second most influential greenhouse gas after CO_2 and responsible for approximately 20% of the warming potential as a result of anthropogenic activities since the start of the Industrial Revolution (Etminan et al., 2016). However, CH_4 is more powerful at trapping radiation. The warming potential of CH_4 is estimated to be 28 times higher than that of CO_2 over a 100-year period and is even more potent over a 20-year period, at 84 times higher (Bridgham et al., 2013; IPCC, 2013). Atmospheric CH_4 concentrations have more than doubled since pre-industrial times, and this upward trend continues to persist (Dlugokencky et al., 2009; Jackson et al., 2020; Nisbet et al., 2019). In 2021, the estimated annual growth rate of atmospheric CH_4 concentration reached a record high since 1984 (Lan et al., 2023) exceeding more than three times the average annual growth rate observed from 2007 to 2015 (Poulter et al., 2017). Such an increase significantly contributes to the radiative forcing of the atmosphere and further amplifies global warming. Moreover, CH_4 has a large natural emission component from permafrost in the northern latitudes. Thawing permafrost initiates a self-reinforcing cycle: initial warming leads to

Visualization: Sandeep Chinta
Writing – original draft: Sandeep Chinta
Writing – review & editing: Xiang Gao, Qing Zhu

increased emissions, which in turn cause further warming and continued thaw. Despite methane's relatively short atmospheric lifetime of 12.4 years (Balcombe et al., 2018), its warming potential makes it an essential cog in the wheel for measures to reduce climate change (Shindell et al., 2012).

CH_4 emissions originate from a broad spectrum of natural and anthropogenic sources. The substantial contributors among anthropogenic sources are agriculture, fossil fuel extraction, and livestock farming (Bridgham et al., 2006; Ciais et al., 2013; Jackson et al., 2020; Kirschke et al., 2013; Saunois et al., 2016). Wetlands contribute to more than 30% of total emissions and are the most significant contributor to emissions among natural sources. Wetlands are diverse ecosystems consisting of swamps, marshes, and rice paddies, enabling CH_4 production through microbial metabolic processes within their anaerobic environments (Bodelier & Laanbroek, 2004; Turetsky et al., 2014). It is challenging to measure and accurately predict CH_4 emission from wetlands due to their intricate nature and spatiotemporal variability (Rosentreter et al., 2021). In addition, the role of wetlands in the total CH_4 budget and their impact on inter-annual variability and changes in the CH_4 growth rate is still poorly understood (Poulter et al., 2017). This issue arises from various factors ranging from soil properties, temperature, vegetation types, and water table dynamics that control CH_4 production, consumption, and transfer in wetlands (Bousquet et al., 2006; Melton et al., 2013). Global warming could aggravate the CH_4 emissions from wetlands as they are susceptible to climatic conditions and land-use changes (Gurevitch & Mengersen, 2019). To address climate change effectively, it is critical that we enhance our ability to model and predict wetland CH_4 emissions. This requires comprehensive, process-based models that encompass all relevant factors and processes.

Biogeochemistry models inherently introduce uncertainties in modeling CH_4 emissions due to several factors. Model uncertainty arises because each biogeochemistry model simplifies real-world processes through a combination of its structure, complexity, physics, usage, and the tuning of model parameters. These simplifications vary considerably among models, leading to a wide range of accuracies in representing methane emission processes. A large number of model parameters relating to diverse physical, biological, and chemical processes associated with CH_4 dynamics induce parameter uncertainty. These parameters generally take fixed values, but they are not unambiguously known and usually must be prescribed based on the best available knowledge. Parameter uncertainty is commonly assessed by sensitivity analysis (SA) based on sampling within the theoretical, plausible ranges of parameters, which is the primary focus of this study (Müller et al., 2015; Ricciuto et al., 2021; Riley et al., 2011). Other sources of uncertainty include spatial variability of wetlands, scarcity of observations for calibration, initial and boundary conditions, and meteorological forcing to drive the model (Papa et al., 2013; Xu et al., 2012).

SA quantifies the influence of different input parameters on the model's output, thus helping to identify which parameters significantly contribute to overall parameter uncertainty. Several studies (Chinta et al., 2021; C. Wang et al., 2020) implemented SA in understanding parameter uncertainties in complex earth system models. Ricciuto et al. (2018) applied SA to the Energy Exascale Earth System Model (E3SM) land model (ELM) parameters with respect to carbon cycle output. Fisher et al. (2019) examined parameter controls on vegetation responses in the Community Land Model (CLM) using SA. Yuan et al. (2021) examined the effects of warming and elevated CO_2 on peatland CH_4 emissions using a similar approach. Ricciuto et al. (2021) used SA to show that production and substrate parameters are vital for regulating temporal patterns of surface CH_4 fluxes. Song et al. (2020a, 2020b) performed SA for a microbial functional group-based CH_4 model and observed that CH_4 emissions are sensitive to the parameters that regulate dissolved organic carbon and acetate production. However, a major challenge in SA is the computational demand for conducting a vast number of ELM simulations (the Monte Carlo method) to efficiently explore the parameter space. This approach is particularly infeasible for complex biogeochemistry models. To address this, machine learning (ML)-based emulators, also known as meta-models or surrogate models, which mimic complex earth system models, are employed. These emulators can approximate model behavior accurately with fewer simulations. Müller et al. (2015) constructed an ML-based emulator using radial basis functions (Gutmann, 2001) for CH_4 parameter estimation in CLM4.5bgc. Dagon et al. (2020) also implemented an emulator using artificial neural networks (Gurney, 2018) in CLM biophysical parameter estimation. Emulators based on Gaussian process regression or kriging (Rasmussen & Williams, 2006) were also applied by Gao et al. (2021) to quantify the sensitivity of soil moisture to uncertain model parameters in CLM.

Although SA and ML have been successfully employed in various areas of earth system modeling, their potential in improving CH_4 emissions modeling still needs to be explored. Our study addresses several primary research

Table 1
Geographical and Vegetation Details of the Simulated FLUXNET-CH_4 Sites

Site ID	Site name	Latitude	Longitude	PFT	PFT name
RU-Fy2	Fyodorovskoye dry spruce	56.45	32.90	1	Needleaf evergreen temperate tree
DE-SfN	Schechenfilz Nord	47.81	11.33	1	
CH-Dav	Davos	46.82	9.86	1	
US-Ho1	Howland Forest (main tower)	45.20	−68.74	1	
US-PFa	Park Falls/WLEF	45.95	−90.27	7	Broadleaf deciduous temperate tree
RU-Cok	Chokurdakh	70.83	147.49	11	Broadleaf deciduous boreal shrub
SE-Deg	Degero	64.18	19.56	12	Arctic c3 grass
DE-Zrk	Zarnekow	53.88	12.89	13	Cool c3 grass
CH-Cha	Chamau	47.21	8.41	13	
DE-Hte	Huetelmoor	54.21	12.18	13	
US-OWC	Old Woman Creek	41.38	−82.51	13	
US-WPT	Winous Point North Marsh	41.46	−83.00	13	
CN-Hgu	Hongyuan	32.85	102.59	13	
US-MRM	Marsh Resource Meadowlands Mitigation Bank	40.82	−74.04	14	Warm c4 grass

questions, including: (a) which critical parameters dominate the sensitivity of various model-simulated CH_4 emissions? (b) what are temporal (seasonal vs. annual) and spatial (site-to-site or vegetation type to vegetation type) characteristics of such parametric sensitivity? and (c) is there any potential to improve model-simulated methane emissions? We integrated various advanced techniques to tackle these scientific questions. SA is employed to examine the influence of different input parameters on various components of CH_4 emissions, while ML is used to emulate the ELM biogeochemistry model with feasible computational cost desired by global SA.

2. Methodology

2.1. FLUXNET-CH_4 Data for Wetland CH_4 Emission

FLUXNET-CH_4 is a global network of sites that provides continuous, high-frequency, and quality-checked eddy covariance CH_4 flux measurements (Delwiche et al., 2021; Knox et al., 2019). This data helps get a deeper understanding of the variability of CH_4 emissions worldwide and also help validate CH_4 emissions from biogeochemistry models. The network currently encompasses 81 sites across various vegetation types. From the initial 81 sites, we excluded crop sites due to the complexities introduced by irrigation management, such as quantifying the volume of water required for irrigation. Additionally, sites with less than 2 years of continuous observational data were omitted. Considering the computational expense of simulating all locations, we chose a subset of sites in our study with a diverse mix of vegetation types across various climate zone classifications.

Table 1 presents the list of 14 sites selected for this study, along with their locations and vegetation types. The geographical locations of these sites are presented on a map in Figure S1 of Supporting Information S1. The vegetation types include needleaf evergreen temperate tree (NETT, 4 sites), broadleaf deciduous temperate tree (BDTT, 1 site), broadleaf deciduous boreal shrub (BDBS, 1 site), arctic c3 grass (AC3G, 1 site), cool c3 grass (CC3G, 6 sites), and warm c4 grass (WC3G, 1 site). The PFT number corresponds to that specified in the ELM biogeochemistry model. The corresponding Köppen climate classification of the 14 FLUXNET-CH_4 sites is provided in Table S1 of Supporting Information S1.

2.2. Model Description and Parameter Selection

The Energy Exascale Earth System Model (E3SM) land model version 2 (ELMv2) (Golaz et al., 2022) is used in this study, which is branched from Community Land Model (CLM) version 4.5 (CLM4.5) (Oleson et al., 2013). The model underwent several updates associated with the biogeochemical representation of global carbon, nitrogen, and phosphorus cycles (Zhu et al., 2019). Some of the other relevant updates include the introduction of the multiple agent nutrient competition, dynamic allocation, modifications to the photosynthesis physiology

scheme, N_2 fixation, and phosphatase modules. Several studies (Golaz et al., 2019, 2022; Ricciuto et al., 2018) described these updates from CLM4.5 in great detail. The CH_4 biogeochemistry model (Riley et al., 2011) explicitly represents several processes, such as CH_4 production, ebullition, aerenchyma transport, aqueous and gaseous diffusion, CH_4 oxidation, and mass balance for unsaturated and saturated soils with the following governing equation:

$$\frac{\partial(RC)}{\partial t} = \frac{\partial F_D}{\partial z} + P(z,t) - E(z,t) - A(z,t) - O(z,t) \quad (1)$$

where R represents gas in aqueous and gaseous phases, C represents the concentration of CH_4 with respect to water volume (mol m^{-3}), F_D represents aqueous and gaseous diffusion (mol m^{-2} s^{-1}), P represents CH_4 production (mol m^{-3} s^{-1}), E represents ebullition (mol m^{-3} s^{-1}), A represents aerenchyma transport (mol m^{-3} s^{-1}), O represents oxidation (mol m^{-3} s^{-1}), z represents vertical dimension (m), and t represents time (s). The model indirectly accounts for the role of wetland plant functional types (PFTs) in methane production by using heterotrophic respiration rates as a proxy. While wetland PFTs are not explicitly represented, their influence is captured through the impact they have on the soil's organic carbon content, which is a key determinant of heterotrophic respiration. This respiration, primarily driven by microbial activity decomposing organic matter, provides a substrate for methanogenesis. These rates, in turn, are adjusted for environmental factors like soil temperature, pH, and redox potential, which are critical in determining the actual availability of substrates for methane production, hence linking PFTs to methanogens. Ebullition occurs when the CH_4 partial pressure, as a function of temperature and depth below the water table, exceeds 15% of the local pressure. Bubbles are added to the saturated columns' surface flux and placed immediately above the water table interface in unsaturated columns. Aerenchyma transport is modeled as gaseous diffusion driven by a concentration gradient between the specific soil layer and the atmosphere and, if specified, by vertical advection with the transpiration stream. CH_4 oxidation is represented with double Michaelis–Menten kinetics (Arah & Stephen, 1998), dependent on the gaseous CH_4 and O_2 concentrations. Gaseous diffusivity in soils depends on temperature-dependent molecular diffusivity, soil structure, porosity, and organic matter content. Aqueous diffusivity in the saturated part of the soil depends on temperature-dependent molecular diffusivity and porosity. Gaseous diffusion is assumed to dominate above the water table interface and aqueous diffusion below it.

These processes in the CH_4 biogeochemistry model are represented as functions of climate, vegetation, soil conditions, and empirical parameters. The default values of these parameters are typically assigned based on the best available knowledge from a limited experimental or theoretical investigation. The parameter selection in our study is based primarily on the 16 major parameters affecting ELM's methane biogeochemistry as identified by Riley et al. (2011). From this list, we exclude parameters related to pH and redox potential, as they are assigned static values and thus have a negligible impact on the temporal dynamics of CH_4 emissions. The seasonal inundation factor within the wetland inundation fraction parameterization is also omitted. The minimum and maximum thresholds to initiate and terminate ebullition are maintained at fixed values of 0.15. To simplify our calibration, we concentrate exclusively on $C_{e,\max}$. We adopted 12 of the 16 parameters from Riley et al. (2011). As previously mentioned, ELM's CH_4 production utilizes soil heterotrophic respiration flux as a proxy for methanogen CO_2 substrate availability. Therefore, it is crucial to also test the sensitivity of CH_4 emissions to soil respiration parameters. The selection of these respiration parameters is guided by Koven et al. (2013), which includes all seven turnover parameters (representing substrate availability) of the century-type soil decomposition cascade. Table 2 presents the 19 ELM parameters used in this study, which pertain to various processes such as production, substrate availability, ebullition, diffusion, aerenchyma transport, and oxidation. For parameters with an unknown uncertainty range, ±50% of the default value is used.

2.3. Numerical Experiment Design

Site-level single-point ELM simulations are performed for the 14 FLUXNET-CH_4 sites. Each simulation follows the same 3-step modeling protocol. In the first step, an accelerated spin-up (as described in Ricciuto et al. (2018)) is performed for 300 years with CO_2 concentration set to the value of the year 1901. Climatic Research Unit and Japanese reanalysis (CRU JRA) v2.2 data (Harris, 2021) at a six-hourly frequency and 0.5° × 0.5° resolution is used for meteorological forcing. For each site, forcing data from the nearest grid point is used. The forcing data and N_2 depositions are cycled over the years 1901–1920. The second step involves a regular spin-up for 200 years

Table 2
List of 19 ELM Parameters Used and Their Default Values, Ranges, and Brief Description

Mechanism	Parameter	Default	Range	Units	Description
Production	Q_{10}	2	[1.5 4]	-	CH_4 production Q_{10}
	β	0.2	[0.1 0.3]	-	Effect of anoxia on decomposition rate
	f_{CH_4}	0.2	[0.1 0.3]	-	Ratio between CH_4 and CO_2 production below the water table
Substrate availability	z_τ	0.5	[0.1 0.8]	m	e-folding depth for decomposition
	τ_{cwd}	3.33	[2 20]	$Year^{-1}$	Corrected fragmentation rate constant CWD
	τ_{l1}	0.054	[0.027 0.081]	Year	Turnover time of litter 1
	$\tau_{l2\text{-}l3}$	0.204	[0.102 0.306]	Year	Turnover time of litter 2 and litter 3
	τ_{s1}	0.137	[0.0685 0.2055]	Year	Turnover time of soil organic matter (SOM) 1
	τ_{s2}	5	[0.0685 0.2055]	Year	Turnover time of soil organic matter (SOM) 2
	τ_{s3}	222.22	[111.11 333.33]	Year	Turnover time of soil organic matter (SOM) 3
Ebullition	$C_{e,\max}$	0.15	[0.075 0.225]	mol m^{-3}	CH_4 concentration to start ebullition
Diffusion	f_{D_0}	1	[1 10]	m^{-2} s^{-1}	Diffusion coefficient multiplier
Aerenchyma	p	0.3	[0.15 0.45]	-	Grass aerenchyma porosity
	R	2.9×10^{-3}	$[1.45 \times 10^{-3}\ 4.35 \times 10^{-3}]$	m	Aerenchyma radius
	r_L	3	[1.5 4.5]	-	Root length to depth ratio
	F_a	1	[0.5 1.5]	-	Aerenchyma conductance multiplier
Oxidation	K_{CH_4}	5×10^{-3}	$[5 \times 10^{-4}\ 5 \times 10^{-2}]$	mol m^{-3}	CH_4 half-saturation oxidation coefficient (wetlands)
	K_{O_2}	2×10^{-2}	$[2 \times 10^{-3}\ 2 \times 10^{-1}]$	mol m^{-3}	O_2 half-saturation oxidation coefficient
	$R_{o,\max}$	1.25×10^{-5}	$[1.25 \times 10^{-6}\ 1.25 \times 10^{-4}]$	mol m^{-3} s^{-1}	Maximum oxidation rate (wetlands)

with the same CO_2, N_2 deposition configuration and forcing data as in accelerated spin-up but without accelerating soil turnover. The third step is a 120-year transient run from 1901 to 2020. This step utilizes time-varying historical CO_2 concentrations and CRU JRA forcing data and nitrogen depositions of the years 1901–2020. Each three-step simulation, spanning from the accelerated spin-up to the transient run, took 6 CPU hr on a single core of an Intel Broadwell E5-2697A v4 CPU (2.60 GHz), using approximately 4 GB of the 128 GB RAM allocated to a 32-core node. Five model output variables are considered for sensitivity analysis: CH_4 emission, CH_4 production, diffusive surface CH_4 flux, ebullition surface CH_4 flux, and aerenchyma surface CH_4 flux. The values of these fluxes are averaged for 2001–2020. CH_4 emission is the sum of diffusion, ebullition, and aerenchyma surface fluxes. To provide an overview of the methodology before discussing the details, Figure 1 presents a flowchart of the processes implemented in this study.

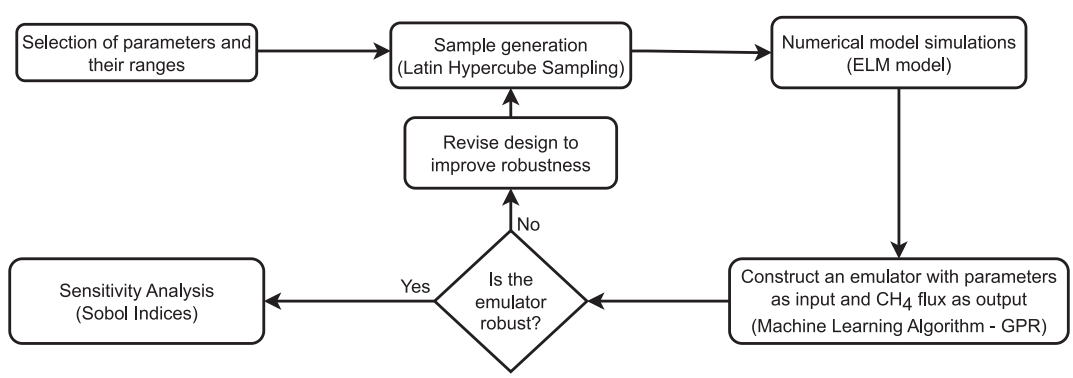

Figure 1. Flowchart of the methodology implemented showing the main steps and sequence of operations.

2.4. Gaussian Process Regression-Based Emulators

Gaussian process regression (GPR), a machine learning algorithm, is employed to develop an emulator that approximates the model behavior. GPR is widely used as an emulator due to its robustness and flexibility (Rasmussen & Williams, 2006; J. Wang, 2020). This algorithm is particularly suitable when the relationship between inputs and output is complex and non-linear. Several studies (Baki et al., 2022b; Chinta & Balaji, 2020; Gong et al., 2015; C. Wang et al., 2014) established the superiority of GPR as an emulator for earth system models compared to other ML algorithms. GPR is defined by the mean function, $m(x)$, and covariance function, $k(x,x')$, where x and x' are points in the input space. The expected value of the function at point x is given by the mean function, whereas the covariance function gives the correlation between the function values at two different points. For a Gaussian process $f(x) \sim GP(m(x),k(x,x'))$, the joint distribution of any finite number (n) of function values $f = [f(x_1),f(x_2),...,f(x_n)]^T$ follows a multivariate Gaussian distribution:

$$P(f|X) = \mathcal{N}(f|\mu,K) \tag{2}$$

where X is the observations or training data, $\mu = [m(x_1),m(x_2),...,m(x_n)]^T$ is the mean vector, and K is the covariance kernel matrix with $K_{ij} = k(x_i,x_j)$.

The main advantage of GPR is the presence of a covariance function, which helps encode our assumptions about the function to be learned. The mean function is typically set to a constant value, often zero or the average of the training data. For our study, we standardize the outputs of ELM to have an average of zero. Standardization is done by computing the mean and standard deviation of the entire training data set, then subtracting the mean and dividing by the standard deviation for each data point. The resulting training data will have a mean of 0 and a standard deviation of 1. This step is crucial to ensure the stability and accuracy of our analysis. GPR has several options to choose from for a covariance kernel function. We employed one of the widely used kernel functions in our analysis, which combines a constant kernel with a radial basis function (RBF) kernel. This kernel function can be mathematically represented as:

$$k(x,x') = \sigma_f^2 \exp\left(-\frac{1}{2\ell^2}\|x - x'\|^2\right) \tag{3}$$

where x and x' represent two points in the input space, the two hyperparameters for this kernel are σ_f^2 (signal variance) and l (length-scale). The signal variance controls the average distance of function values from their mean, while the length scale determines the smoothness of the function. This kernel function provides the GPR with the flexibility to capture complex patterns in the data. The hyperparameters of the kernel function can be learned from the training data using such techniques as maximum likelihood estimation. Once validated, the trained GPR emulator can not only predict the corresponding output for a new point in the input space but also quantify the degree of uncertainty in this prediction. This is a decisive advantage of GPR over other ML algorithms.

Emulators were designed to take 19 parameter values as input and produce five CH_4 flux values as outputs. For each of the five CH_4 fluxes, an individual emulator was developed at every site, resulting in a total of five emulators per site. To generate the training data for emulators at each site, a total of 190 simulations were performed with different combinations of parameter values. The selection of 190 simulations aligns with the guidelines proposed by Loeppky et al. (2009) that a training data size of 10 times the number of parameters (19) is sufficient to construct a robust emulator. The parameters were not altered individually but were collectively modified instead in each simulation to represent different scenarios within the model's parameter space. These 190 sets of parameter combinations were generated using Latin Hypercube Sampling (LHS), a technique that effectively and efficiently samples a multidimensional distribution of parameters (McKay et al., 1979) across given parameter ranges (Table 2). LHS is recognized as superior to simple random sampling, particularly in scenarios with a large number of dimensions (Iman et al., 1981). It offers improved representativeness and efficiency in parameter sampling, ensuring a more uniform and thorough exploration of the parameter space.

The emulators were constructed using the training data from the 190 ELM simulations. A single prediction from a GPR emulator was achieved in just 0.72 milliseconds, in contrast to the 6 CPU hr required for the actual

simulation. To assess the adequacy of the emulator at untried points, an additional 50 sets of LHS parameter values are sampled, and corresponding ELM model simulations are performed at each site to test the performance and robustness of the constructed emulator. We use the coefficient of determination, R^2, between the model-simulated and emulator-estimated CH_4 fluxes as the evaluation metric. The closer to 1 the values are, the more accurate the emulator is. Once the emulator was validated, it was used for performing SA.

2.5. Sobol Sensitivity Analysis

The Sobol sensitivity analysis method (Sobol, 2001), a variance-based approach to identify the sensitive model parameters, is used in this study. This method was successfully implemented in several studies (Baki et al., 2022a; Gao et al., 2021; Reddy et al., 2023; Ricciuto et al., 2018) to conduct SA for various Earth system model parameters. The Sobol method decomposes the total variance in the model output, with each flux considered separately, into variances corresponding to input parameters. There are two essential features of this method. First, it is a global method, as the sensitivity is evaluated across the whole input parameter space. Second, this method can quantify the primary or first-order effects of sensitivity for each parameter and the interaction effects between parameters. These features ensure a comprehensive understanding of the sensitivity analysis of the parameters is obtained.

The total output variance, V, is decomposed as

$$V = \sum_{i=1}^{n} V_i + \sum_{1<i<j<n} V_{i,j} + \ldots + V_{123\ldots n} \tag{4}$$

where n is the total number of parameters. The total output variance V is systematically decomposed into individual and interactive components. First, we account for the variances attributed to each parameter independently, denoted as V_i for the ith parameter. Then, we consider the variances resulting from the pairwise interactions between parameters, represented as V_{ij} for the interactions between ith and jth parameters. This process hierarchically accounts for increasingly complex interactions among groups of parameters, culminating in $V_{123\ldots n}$, which represents the variance from the interaction of all n parameters together. This method ensures that the total variance V encapsulates not only the individual effects of each parameter but also the collective influence of their interactions at different levels. As shown below, the Sobol indices are obtained by dividing the respective variances by the total variance.

$$S_i = \frac{V_i}{V}; \quad S_{ij} = \frac{V_{ij}}{V}; \quad \ldots; \quad S_{12\ldots n} = \frac{V_{12\ldots n}}{V} \tag{5}$$

where S_i is the Sobol index for the first-order (main) effect from the ith parameter. Total order Sobol index of ith parameter, which is the sum of its main and all interaction effects, S_{Ti} is given as:

$$S_{Ti} = S_i + S_{ij} + \ldots + S_{12..i..n} \tag{6}$$

Despite the detailed insights provided, this method requires multiple model runs to cover the entire parameter space for estimating the sensitivity indices accurately (Saltelli et al., 2008). GPR emulators developed in the previous steps were used to evaluate the main and total sensitivity indices for the five CH_4 fluxes at different sites using the Sobol method. This decomposition of the total effects of each parameter into main and interaction effects is a critical attribute of the Sobol SA method, enhancing our understanding of parameter sensitivity across various contexts.

2.6. Metrics for Comparing Simulated Emissions With FLUXNET-CH_4 Measurements

It is important to understand how the simulated emissions from perturbed parameter sets compare with observed emissions. The model simulated monthly-averaged CH_4 emissions from the 190 parameter sets are compared against FLUXNET-CH_4 observations at each site, and root mean square error (RMSE) is evaluated.

$$RMSE = \sqrt{\frac{\sum_{t=1}^{T} (sim^t - obs^t)^2}{T}} \quad (7)$$

where sim^t and obs^t are the simulated and observed values of monthly CH_4 emission from the simulated site at time t, respectively. T is the number of months. We calculated a normalized root mean square error (nRMSE) for each of the 190 initial sets of parameter values. This normalization was performed by comparing each nRMSE to the RMSE obtained from the default parameter run. The nRMSE for a given set, i, is computed as:

$$nRMSE_i = \frac{RMSE_i}{RMSE_{def}} \quad (8)$$

In this equation, $RMSE_i$ represents the RMSE for the specific set of parameter values, while $RMSE_{def}$ denotes the RMSE derived from the simulation with default parameter values. A parameter set with an nRMSE value less than one indicates improved performance (lower RMSE) in comparison to the default.

3. Results

3.1. Sensitivity Analysis - Main Effects and Interaction Effects

Emulators for five CH_4 fluxes (CH_4 emission, CH_4 production, diffusive surface CH_4 flux, ebullition surface CH_4 flux, and aerenchyma surface CH_4 flux) were developed at each site using the initial 190 simulations. These emulators were then evaluated by comparing the emulator-predicted fluxes with the ELM-simulated counterparts from 50 independent test simulations at each site. We present results for one of the sites, specifically the CH-Cha site (PFT-13: Cool c3 grass), as shown in Figure 2. The emulators performed well for all the fluxes with R^2 values ranging from 0.84 to 0.95. Similarly, for fluxes at other sites, the emulators also performed reasonably well, with R^2 values above 0.80, as shown in Figure S2 of Supporting Information S1. Overall, the emulator captures well the model behavior for various fluxes across the entire parameter uncertainty space over the sites with different vegetation types and is considered to be accurate and robust. Therefore, the GPR-based emulators can be reliably applied to derive the Sobol SA indices and further quantify the main and interaction effects of the fluxes relative to each parameter.

The main effect (first-order Sobol index) of a parameter represents the influence of that parameter alone on the considered flux, disregarding any interaction effects with other parameters. Heatmaps for two sites, CH-Cha (PFT-13: Cool c3 grass) and SE-Deg (PFT-12: Arctic c3 grass) are displayed in Figure 3. Each cell of the heatmap represents the value of the main effect for its corresponding parameter (x-axis) and flux (y-axis), with the color intensity indicating the strength of the parameter sensitivity. The heatmaps for both sites were remarkably similar, reflecting parallel sensitivity trends across the parameters at these two sites. The CH_4 production parameters Q_{10} and f_{CH_4} (ratio between CH_4 and CO_2 production below the water table) displayed pronounced sensitivity for all fluxes. The diffusion parameter f_{D_0} (diffusion coefficient multiplier) was a predominantly sensitive parameter for diffusion, whereas the oxidation parameters $R_{o,\max}$ (maximum oxidation rate—wetlands) and K_{CH_4} (CH_4 half-saturation oxidation coefficient—wetlands) emerged as sensitive parameters for aerenchyma transport across these two sites. Apart from these five parameters, the remaining parameters had negligible influences on all fluxes for these two sites. Results corresponding to other sites are presented in Section 3.2. Figure 4 illustrates the total effect Sobol indices, encapsulating main (blue) and interaction effects (red), for various CH_4 fluxes relative to each parameter at the two sites mentioned above. The main effect values are the same as those represented in the heatmaps (Figure 3). Main effects were more prominent than interaction effects for all parameters, highlighting the dominant influence that individual parameters exert on the different CH_4 fluxes. For all fluxes at these two sites, no parameter exhibited a higher interaction effect value compared to its main effect. Other sites share a similar characteristics of total effects (not shown).

3.2. Sensitivity for Multiple Sites Across Vegetation Types

Figure 5 illustrates the distribution of main effect sensitivity indices for each parameter, corresponding to different CH_4 fluxes across the 14 FLUXNET-CH_4 sites. These boxplots comprehensively represent the variation

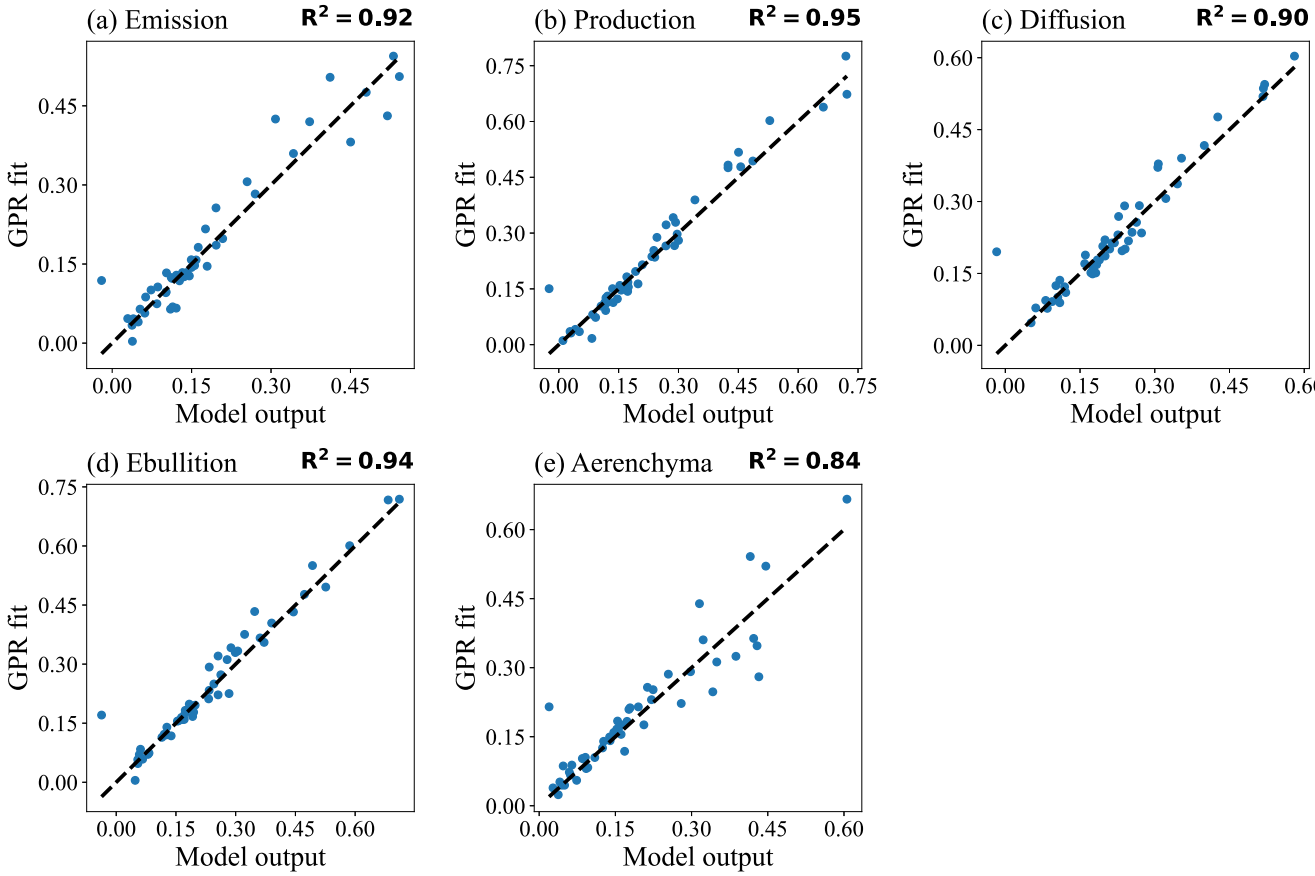

Figure 2. Accuracy of the GPR model based on test data (50 independent simulations) for different CH_4 fluxes at the CH-Cha site (PFT-13: Cool c3 grass). The horizontal axis denotes the model output, and the vertical axis represents the GPR fit.

in sensitivity indices for multiple sites across vegetation types. The production parameter Q_{10} has the highest sensitivity among the parameters for all the fluxes, suggesting its significant role in modulating various CH_4 fluxes. Q_{10} also presents the overall largest variability (inter-site spread) in sensitivity across all the fluxes except for emission, suggesting that the sensitivity of Q_{10} may be highly dependent on climate conditions (geographical locations) and vegetation types. Another production parameter f_{CH_4} was also found to be a fairly sensitive parameter for all the fluxes. In contrast to the earlier heatmaps for CH-Cha and SE-Deg (Figure 3) where f_{D_0} did not influence emission, it was a sensitive parameter with even higher sensitivity than Q_{10} for some sites. The diffusion flux was sensitive to the diffusion parameter (f_{D_0}). Apart from these three parameters, other parameters like $R_{o,\max}$, K_{CH_4} were sensitive parameters for aerenchyma. Additionally, z_τ (e-folding depth for decomposition) was a sensitive parameter for some fluxes (Figures 5b, 5d, and 5e). Also, some parameters (f_{D_0} and $R_{o,\max}$ in Figure 5c) were sensitive at one or two sites, represented as outliers in the figure. It is important to note that roughly 13 parameters consistently showed negligible influence on various fluxes with little inter-site variability. The heterogeneity of CH_4 flux dynamics and associated parametric sensitivities is underscored by the inter-site spread and the presence of outliers in sensitivity indices across the sites. These characteristics underline the heterogeneity of CH_4 flux dynamics and associated parametric sensitivities across the sites (vegetation types). Further examination of parametric sensitivities at additional sites with similar vegetation types may provide a more generalized understanding of these patterns.

3.3. Contribution of Parameters to Variance in CH_4 Fluxes

Figure 6 shows the contribution of different parameters to the variance in CH_4 fluxes at the 14 FLUXNET-CH_4 sites, grouped by the vegetation types. Only those parameters that contribute a minimum of 5% to the variance at any site have been included in the analysis. The results are in agreement with those shown in Figure 5, with the

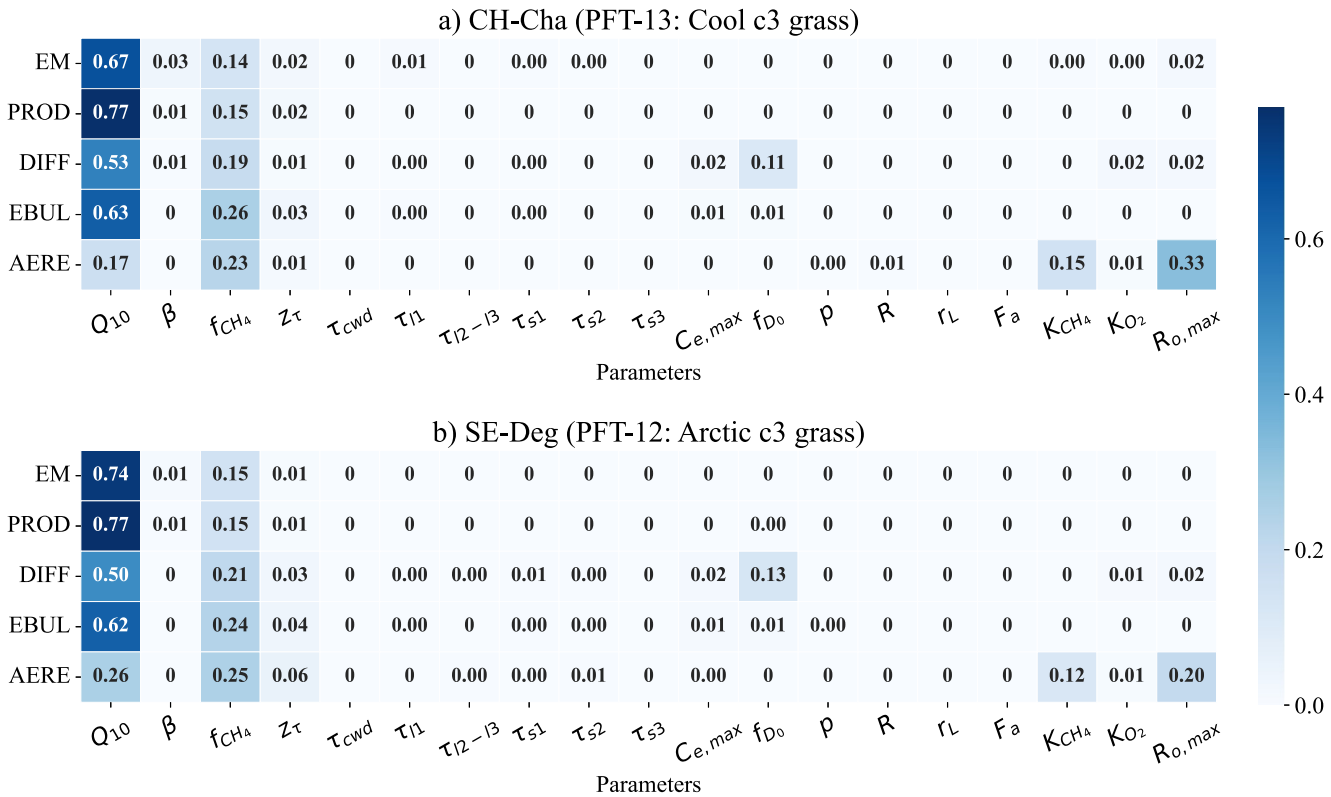

Figure 3. Heat map of main effect sensitivity indices for different CH_4 fluxes (EM: Emission, PROD: Production, DIFF: Diffusion, EBUL: Ebullition, AERE: Aerenchyma) with respect to 19 parameters (shown in Table 1) at (a) CH-Cha and (b) SE-Deg sites.

production parameters Q_{10} and f_{CH_4}, along with the diffusion parameter f_{D_0} being the most influential parameters for different CH_4 fluxes across multiple sites. Some sites had a combination of Q_{10} and f_{CH_4} as sensitive parameters for emission, whereas other sites had f_{D_0} and K_{O_2} as sensitive parameters. The production parameters Q_{10} and f_{CH_4} emerged as sensitive parameters for production at all sites. Apart from these two parameters, substrate availability parameters z_τ, $\tau_{l2\text{-}l3}$ (turnover time of litter 2 and litter 3), and τ_{s2} (turnover time of soil organic matter 2) emerged as sensitive parameters for production at some sites. Theoretically, substrate availability plays an important role in methane production as it determines the quantity and rate at which methanogenic microbes produce methane in anaerobic conditions. The diffusion parameter f_{D_0} and the production parameters Q_{10} and f_{CH_4} emerged as sensitive parameters for diffusion at most of the sites. $R_{o,\max,}$ and z_τ emerged as sensitive parameters for diffusion at some sites. Ebullition was sensitive to the production parameters Q_{10} and f_{CH_4} at most sites. Ebullition parameter, $C_{e,\max}$ (CH_4 concentration to start ebullition), and aerenchyma parameters R (aerenchyma radius) and F_a (aerenchyma conductance multiplier) emerged as sensitive parameters for ebullition at some sites. Although R primarily affects aerenchyma, when aerenchyma and ebullition are dominant pathways for CH_4 to escape, a change in R will affect how much CH_4 is emitted through aerenchyma, and consequently, the amount of CH_4 left over for emission through ebullition. The production parameters Q_{10} and f_{CH_4}, oxidation parameters $R_{o,\max}$, K_{CH_4} and aerenchyma parameter R were sensitive parameters for aerenchyma at most of the sites.

Although some parameters are relevant to a particular process, they could still affect other processes through competition and feedback, depending on the coexistence of certain processes at the time of calculation. The sensitivity can be explained in groups. First, it is reasonable to see production-related parameters dominate the sensitivity because CH_4 production is the biggest flux and directly determines how much CH_4 will be available to emit. Then we see oxidation parameters sometimes show up as sensitive parameters because oxidation sometimes is ignorable (saturated condition) but sometimes could consume a large fraction of newly produced CH_4 (partially saturated). The third group is emission pathway parameters, ebullition, diffusion, and aerenchyma are three emission pathways determined by environmental conditions, vegetation activity, and vertical concentration

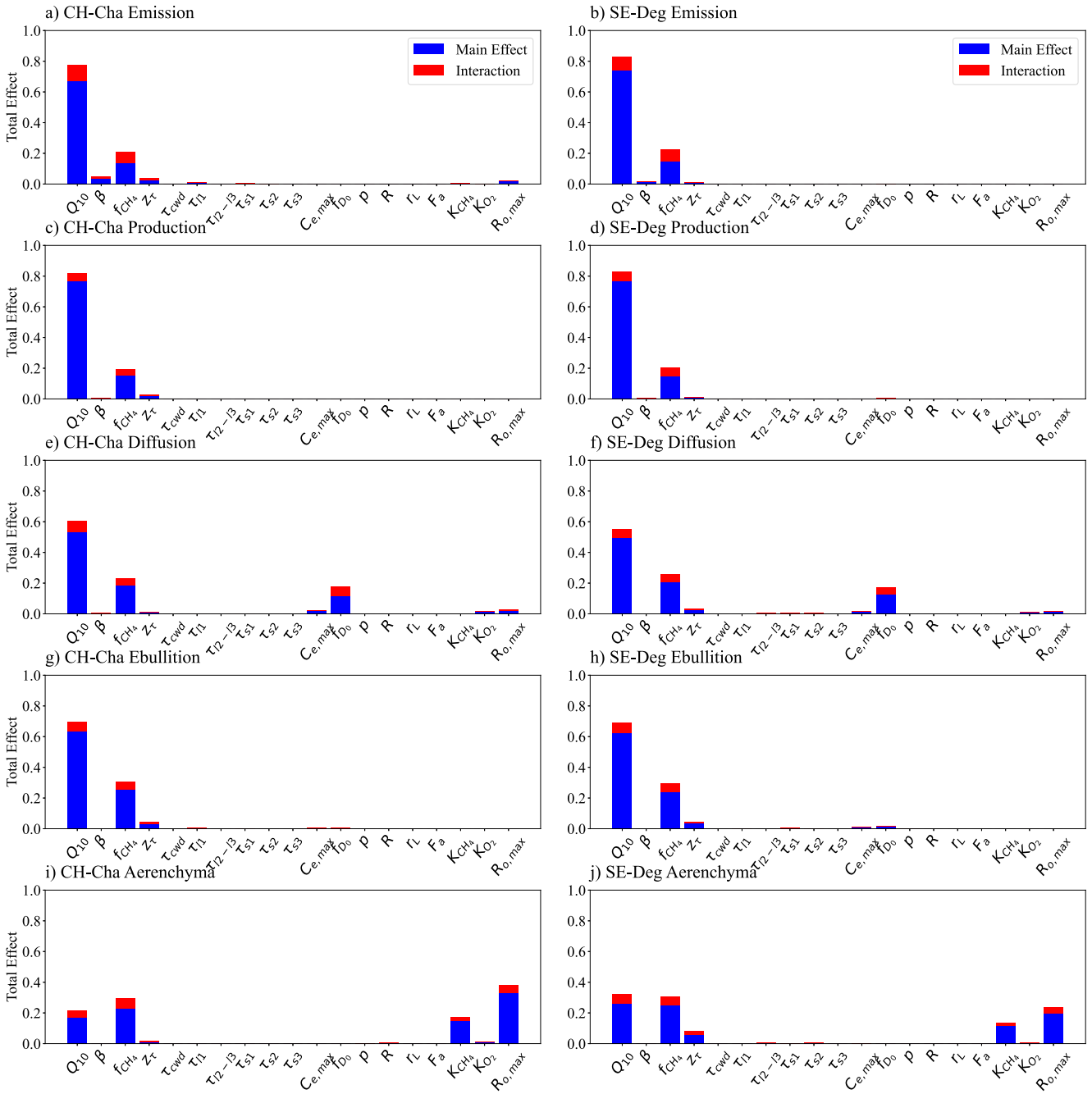

Figure 4. The main effects and interaction effects (differences between the total and main effects) of 19 parameters for different CH_4 fluxes for two sites CH-Cha (PFT-13: Cool c3 grass) and SE-Deg (PFT-12: Arctic c3 grass).

gradient. These three pathways are either dynamically competing or totally independent, depending on whether an emission pathway is favored under certain conditions like vegetation or climate zones.

Across all sites, the top 5 or 6 parameters (parameters with high sensitivity for a particular flux) typically accounted for over 90% of the variance in CH_4 fluxes. However, in certain instances, even fewer parameters were responsible for a substantial portion of the variance. Notably, 13–14 parameters consistently showed a negligible effect on the CH_4 fluxes across these sites. For the four sites characterized by PFT-1 vegetation (Needleleaf evergreen temperate tree), the sensitive parameters remained largely consistent. This consistency prevailed irrespective of the individual climate classifications of these sites (as detailed in Table S1 of Supporting

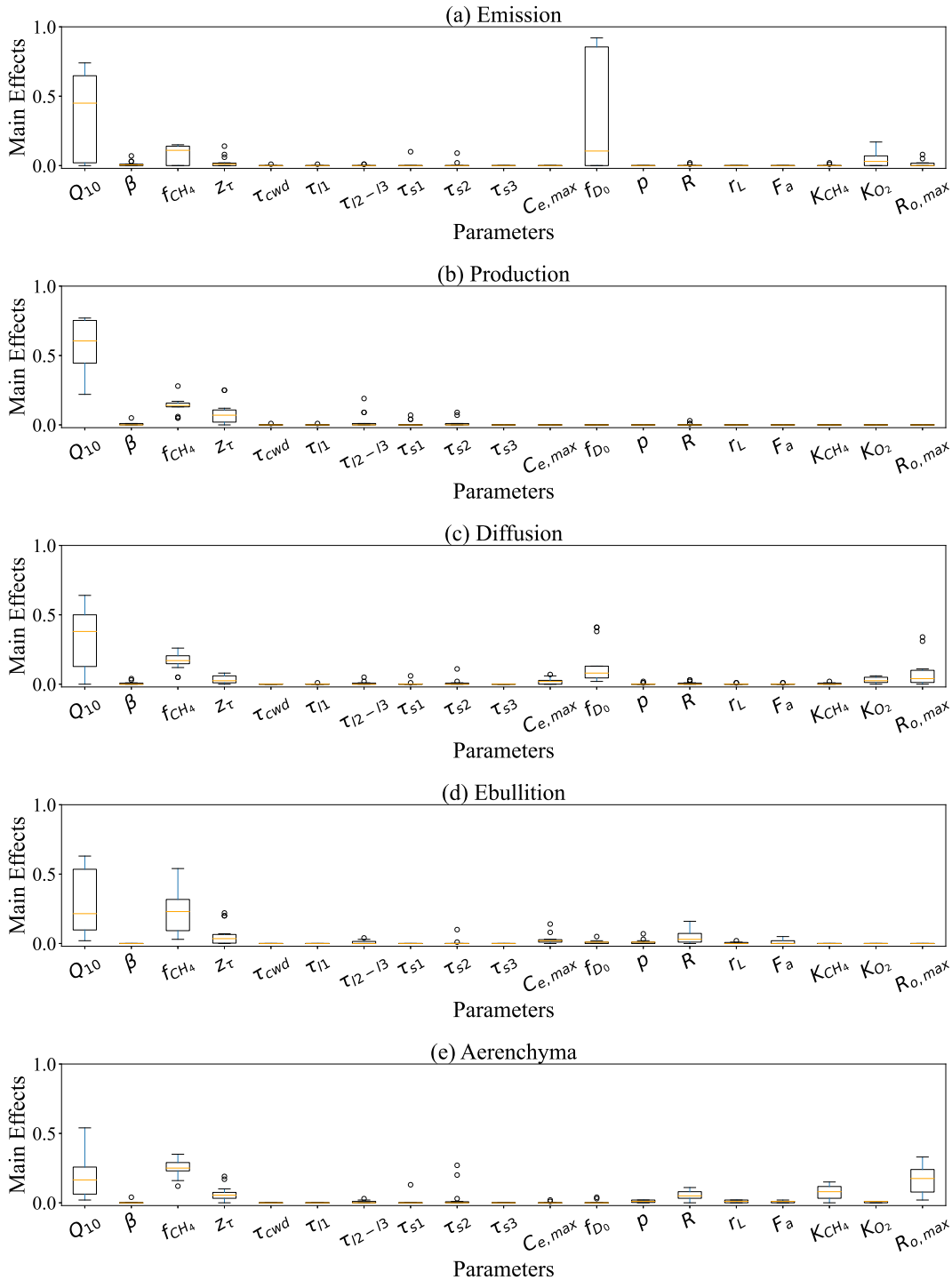

Figure 5. Boxplots showing the distribution of main effect sensitivity indices for each parameter across 14 FLUXNET-CH_4 sites. The boxplot shows the median (orange line), interquartile range, minimum, and maximum after excluding outliers. An outlier, represented by a circle, is a data value outside 1.5 times the interquartile range above the upper quartile and below the lower quartile.

Information S1). This observation implies that, for Needleleaf evergreen temperate tree sites, the climate classification has minimal impact on parameter sensitivity. In contrast, the six sites with PFT-13 vegetation (Cool C3 grass) displayed more variability. While the first three of these sites shared a common sensitivity pattern, the next three differed in their sensitivities. This variation can be linked to their respective climate classifications as the

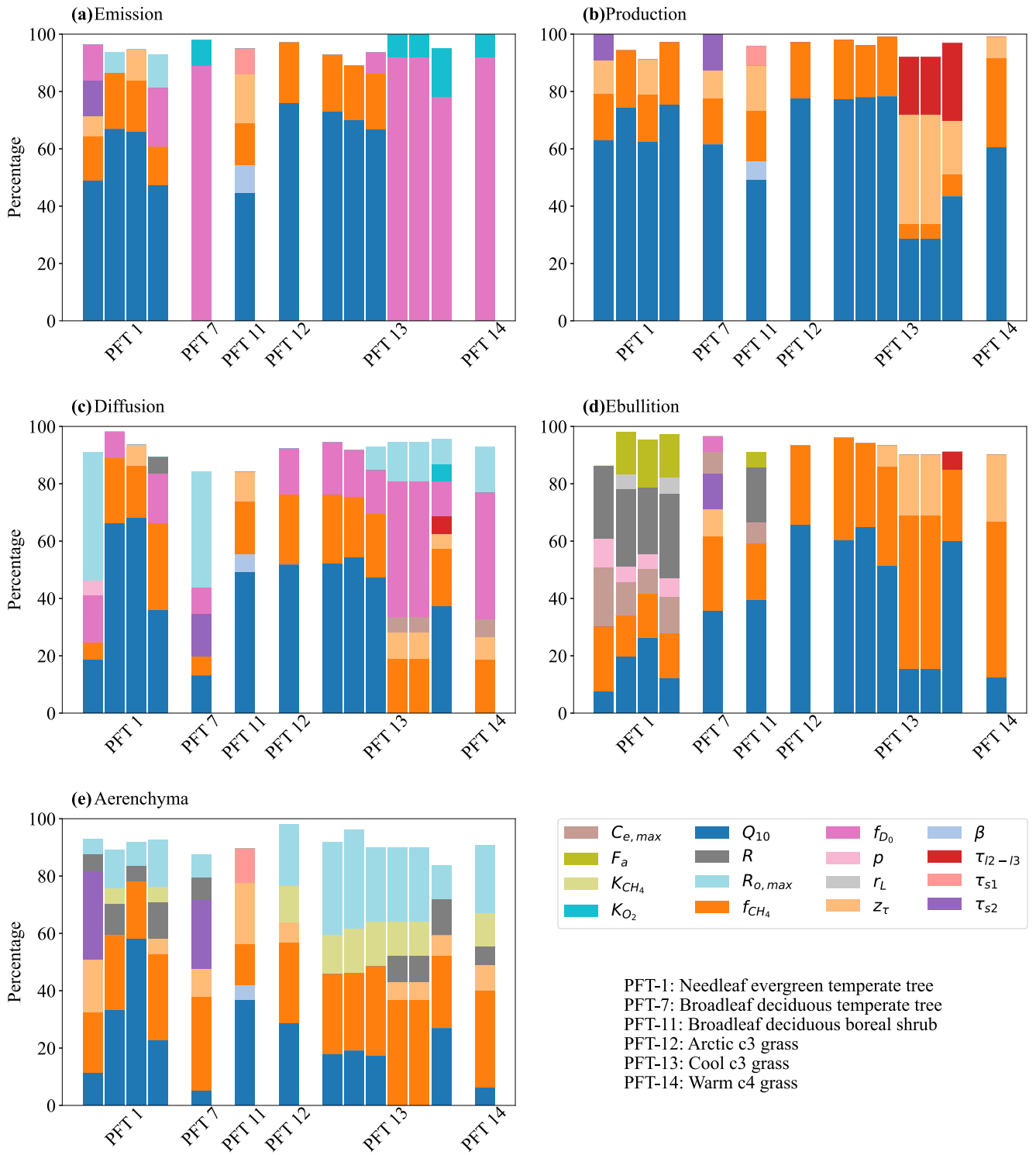

Figure 6. Total effect sensitivity indices of parameters in the percentage of the variance in various CH_4 fluxes, grouped by vegetation types of 14 FLUXNET-CH_4 sites. Only those parameters with at least 5% contribution at any site are included. The height of each color represents the percentage of the total effect Sobol index of that parameter with respect to the sum of the total effect Sobol indices of all parameters at that site, namely, the percentage of the total variance in CH_4 fluxes attributable to that parameter, including its interactions with other parameters. The sites (each bar) in the subfigures are ordered as presented in Table 1, which is PFT 1 (RU-Fy2, DE-SfN, CH-Dav, US-Ho1), PFT 7 (US-Pfa), PFT 11 (RU-Cok), PFT 12 (SE-Deg), PFT 13 (DE-Zrk, CH-Cha, DE-Hte, US-OWC, US-WPT, CN-Hgu), PFT 14 (US-MRM).

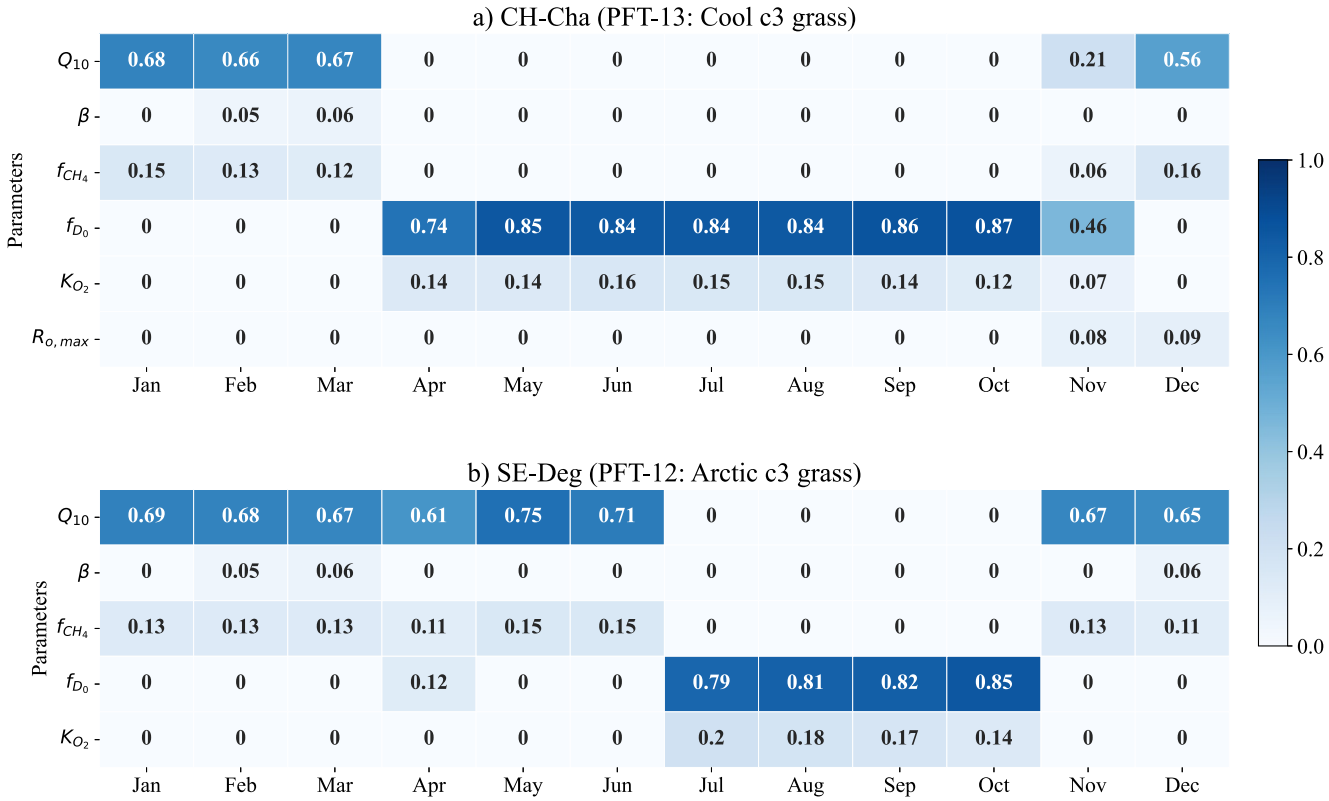

Figure 7. Monthly fluctuation in main effect sensitivity indices of parameters of CH_4 emission for 2 FLUXNET-CH_4 sites. Only those parameters with a minimum value of 0.05 for the main effect (first-order Sobol index) for at least 1 month at the specific site are included.

first three sites are under a temperate climate, and the latter three are categorized as a continental climate. This suggests a stronger influence of climate classification on parameter sensitivity for Cool C3 grass sites.

In light of these findings, it is evident that while vegetation type plays a role in determining parameter sensitivity, climate classification can modulate this effect, especially for certain vegetation types. Further analysis of more sites with the same vegetation types, particularly for the vegetation types with only one site in our study, is necessary to gain a more solid understanding of how a combination of climate conditions and vegetation types affect parametric sensitivity.

3.4. Seasonal Characteristics of Parametric Sensitivity in CH_4 Emission

Given the established seasonal variability in methane emissions from wetlands (Knox et al., 2021; Sakabe et al., 2021; Zhang et al., 2020), we are interested in how the parametric sensitivity of methane emissions fluctuates across months. Figure 7 shows the monthly variation in the main effects of selected parameters for methane emission at two FLUXNET-CH_4 sites, CH-Cha and SE-Deg Parameters with a minimum value of 0.05 for the main effect in at least 1 month were included.

A distinct pattern was observed for the monthly sensitive parameters. For CH-Cha (PFT-13: Cool c3 grass), the production parameters Q_{10} and f_{CH_4} were predominantly sensitive from December to March, whereas for SE-Deg (PFT-12: Arctic c3 grass), their sensitivity extended from November to June. In contrast, during the remaining months, the sensitivity was primarily associated with f_{D_0} and K_{O_2}. The observed monthly fluctuations in parameter sensitivity can be linked to seasonal temperature variations, given that parameters Q_{10} and f_{D_0} are directly temperature-dependent (Riley et al., 2011). Other factors influencing the seasonal variation in methane emissions include gross primary productivity, ecosystem respiration, net ecosystem exchange, latent heat turbulent flux, soil temperature, water table depth, incoming shortwave radiation, and wind direction (Knox et al., 2021). This periodic parameter sensitivity behavior on the month scale is distinctive from the 20-year annual mean in which neither f_{D_0} nor K_{O_2} were dominant sensitive parameters (Figure 3). Long-term averages may obscure some

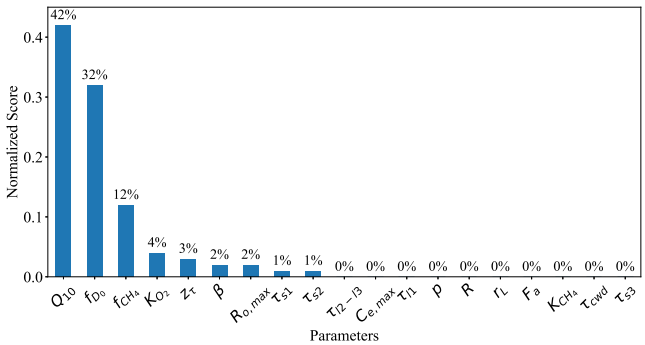

Figure 8. Parameters ranked according to their sensitivity of annually averaged CH_4 emission across 14 FLUXNET-CH_4 sites. The percentage values over each bar represent the normalized score for that parameter.

features inherent in a short temporal scale by smoothing out variations from changing parameter values over shorter durations. Examining monthly averages reveals nuanced parametric sensitivity patterns that might be missed in long-term aggregates.

3.5. Parameter Ranking Based on CH_4 Emission Flux Sensitivity

While Section 3.4 underscores the nuances captured by examining monthly averages, Section 3.5 aims to complement this by offering a broader perspective. Here, we present the hierarchical ranking (Figure 8) of parametric sensitivities to CH_4 emission, derived from the 20-year average across all sites. Although this long-term aggregation potentially smooths over short-term variations, as noted earlier, it serves a crucial different purpose. It allows us to capture overarching trends in parameter sensitivity across the 14 FLUXNET-CH_4 sites corresponding to different vegetation types and climate zones. The total effect Sobol indices of parameters were averaged across all sites to offer a comprehensive perspective on their overall influence across diverse vegetation types. This averaging allows for capturing the general trends in parameter sensitivity and can help in identifying parameters of universal importance. Furthermore, normalizing these averaged values ensures that the results are presented on a consistent scale from 0 to 100, facilitating comparisons. Five parameters Q_{10}, f_{D_0}, f_{CH_4}, z_τ, and K_{O_2} - collectively accounted to approximately 95% of the normalized score, while all the remaining parameters show little to negligible effect on CH_4 emission.

3.6. Comparison of Simulated Emissions With FLUXNET-CH_4 Data

Sensitivity analysis was strictly a modeling exercise designed to understand how different parameters influence a model's output. Comparing the simulated emissions from perturbed parameter sets with observed emissions is essential. This comparison works as an elementary assessment that allows us to understand whether there exists a potential to improve the simulated emissions corresponding to observations by adjusting the parameter values within their ranges. We compared the average monthly ELM-simulated methane emissions from 190 parameter sets to FLUXNET-CH_4 observed emissions at each site (Figure 9a). It is important to note that the observation data available at each site is not across the same timeline (Table S1 in Supporting Information S1). So, the simulated emissions were only compared for the available duration of observations for each site. The ELM simulations over-predicted (under-predicted) the emissions for ten (four) out of the 14 sites. All four sites that under-predicted the emissions belonged to PFT-13: Cool c3 grass. The magnitude of monthly averaged observed emissions varies greatly across sites. A larger range in the emissions resulting from perturbed parameter values indicates greater parameter uncertainty. This variability reflects how sensitive the model's output is to changes in the input parameters, and suggests that the model's predictions could be significantly affected by our confidence in those parameters. This variability in emissions is not uniform across sites. Some sites have higher variability whereas others have lower variability.

A comparison of nRMSE values (Figure 9b) shows that there are always partial parameter sets at each site that have nRMSE values less than 1, indicating an improved performance with lower RMSE compared to using the default parameter values (see Section 2.6 for details). The median nRMSE values were higher than 1 at some sites, such as CH-Dav, RU-Cok, and CN-Hgu, suggesting potential challenges in accurately predicting methane dynamics at these sites. In contrast, sites like US-Ho1, SE-Deg, and DE-Hte-Cha present lower median nRMSE values, indicating improved simulations of CH_4 emissions over the default could be potentially achieved. The minimum nRMSE values, provided in brackets for each site, underscore the extent to which CH_4 emissions with alternative parameters may outperform those with the default at each site, for example, via parameter calibration We also analyze the distribution of RMSE and bias across 190 simulations at each site (Figures S3 and S4 in Supporting Information S1). The values of the identified sensitive parameters can be adjusted within their respective ranges (Table 2) to minimize the difference between the model simulated and the observed CH_4 emissions at each FLUXNET-CH_4 site. This adjustment can be achieved systematically by employing an advanced optimization technique like Bayesian calibration (Gattiker et al., 2016f; Kennedy & O'Hagan, 2001).

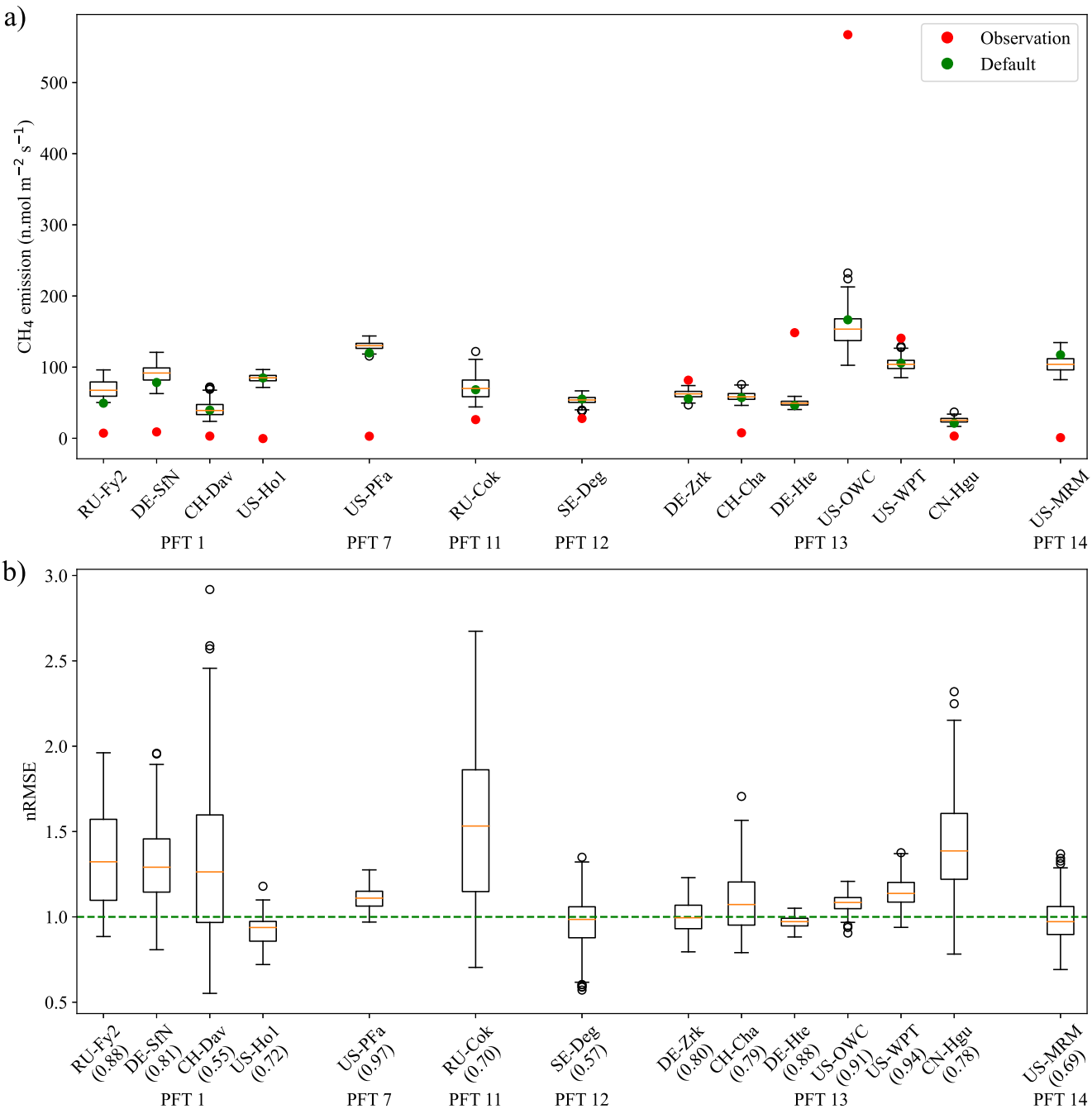

Figure 9. (a) Box plots (190 ELM simulations) depicting the average monthly emission across 14 FLUXNET-CH_4 sites, grouped by their vegetation types. The boxplot shows the median (orange line), interquartile range, minimum, and maximum after excluding outliers and individual circles marking outlier data points. Average monthly emissions of observation (red) and default (green) parameter ELM simulations are also presented. (b) Same as (a) but for nRMSE. The green dashed line signifies an nRMSE value of 1, corresponding to the RMSE from the default parameter simulation for the respective site. The value in brackets below each site label denotes the minimum nRMSE value from a set of 190 simulations for that particular site.

4. Discussion

4.1. Key Parameters Influencing Methane Emission

Sensitivity analysis revealed that five parameters Q_{10}, f_{b_0}, f_{CH_4}, z_τ, and K_{O_2} are among the most sensitive parameters for methane emissions from the chosen wetland sites. Q_{10} represents the temperature-dependent methane production. A higher Q_{10} suggests that an increase in temperature will lead to more methane

production and emissions. This, in turn, can indirectly enhance diffusion, as increased methane production creates larger concentration gradients. The parameter f_{CH_4} is the ratio between CH_4 and CO_2 production below the water table. A higher ratio means a greater dominance of methane in production and emission relative to CO_2. The diffusion coefficient multiplier, f_{D_0}, is equally important. This parameter directly alters the rate of methane movement through gas or liquid. A higher value of f_{D_0} suggests more rapid methane diffusion. As the methane transport increases, it could lead to higher emissions. The e-folding depth, z_r, determines the depth at which microbial decomposition diminishes exponentially. A greater e-folding depth suggests methane production can happen deeper, possibly causing a delay in its release or changing emission patterns due to its travel through various soil and water layers. The parameter K_{O_2} indicates the oxygen concentration at which methane oxidation is halved. Higher K_{O_2} values suggest that more methane is oxidized into CO_2, leading to reduced methane emissions. The minimal impact of the other parameters on CH_4 emissions indicates that while they might be important at specific sites, their overall contribution is less significant when averaged across all sites. This differentiation between universally influential parameters and those with localized effects can guide model developers to focus on the specific sensitive parameters for further improving CH_4 emission modeling based on different research objectives.

Numerous studies have highlighted the sensitive parameters influencing methane emissions. Müller et al. (2015) performed a one-at-a-time sensitivity analysis on 21 parameters within the CLM4.5bgc model, at 16 different sites comprising 6 wetlands and 10 rice paddies. Their findings pointed to Q_{10}, f_{CH_4}, and K_{O_2} as the most sensitive parameters across all sites, with f_{D_0} emerging as sensitive in three specific sites. Similarly, Riley et al. (2011) undertook a sensitivity analysis in the CLM4Me model, identifying Q_{10}, alongside oxidation and aerenchyma parameters, as critical for methane emission. Song et al. (2020a, 2020b) utilized the Sobol sensitivity analysis method for the Integrated Biosphere Simulator (IBIS) model, finding parameters related to production and oxidation to be most influential. Additionally, Zhu et al. (2014) conducted a sensitivity analysis on the TRIPLEX-GHG model, singling out Q_{10} as one of the most sensitive parameters among those examined. These studies collectively underscore the importance of certain key parameters across different models and environmental settings in determining methane emissions. Despite the variation in models, sensitivity analysis methods, and the environmental contexts of the sites considered, there is a consensus in our results and those of other studies regarding the high sensitivity of production and oxidation-related parameters. In our study, the diffusion parameter f_{D_0} emerged as sensitive, which contrasts with its lesser sensitivity in some studies mentioned above. This highlights the nuanced differences in sensitivity analyses and the importance of considering a wide range of parameters and contexts to understand methane emission dynamics fully.

4.2. Scope for Parameter Optimization and Limitations

Adjusting the sensitive parameter values to reduce the simulation error with respect to observations using advanced optimization techniques like Bayesian calibration helps reduce parameter uncertainty. Bayesian calibration involves using Markov Chain Monte Carlo (MCMC) methods to draw multiple parameter samples from the prior distribution, which is usually a uniform distribution. GPR-based emulators are then developed to take the values of sensitive parameters as input and generate the corresponding emission values. The comparison of these outputs with FLUXNET-CH_4 observed emissions, facilitated through an objective function, aids in refining the parameters through an iterative approach (Chinta et al., 2023). After the end of the calibration process, the calibrated parameters are represented by their posterior distributions. Drawing samples from these distributions allows for ensemble simulations that more closely align with observed data. This process significantly improves the model's accuracy and reliability in simulating methane emissions and reduces uncertainty. This step, although not covered in our current study, suggests a significant potential for future research. This approach would foster greater confidence in future CH_4 emission projections, It is important to note that apart from parameter uncertainty, other sources of uncertainty such as uncertainties in forcing data, the accuracy of observational data, and inherent limitations within the model structure could also influence the simulated emissions. Along with aiming to reduce parameter uncertainty using Bayesian calibration, future research could further enhance the accuracy of model simulations by investigating these other forms of uncertainty. This comprehensive examination would contribute to a more robust and reliable modeling approach, ensuring that the simulations more accurately reflect real-world complexities.

This study offers significant insights into the sensitivity analysis of methane emissions. However, several inherent limitations need consideration. The presented results may be dependent on the choice of meteorological forcing data. The spatial scale discrepancy between the model simulations (0.5°) and the point-based observations may also lead to some biases in the results. Despite its computational benefits, the emulator might not fully capture the complex and non-linear dynamics of the ELM biogeochemistry model, potentially leading to minor discrepancies between the emulator's predictions and the actual ELM-simulated outputs. Additionally, using the Monte Carlo approach for generating large samples in the Sobol analysis introduces inaccuracies due to finite sample size (H. Wang et al., 2020). While the monthly fluctuations in parameter sensitivity were examined, the diurnal fluctuations were not explored. Notably, methane emissions exhibit significant diurnal variability (Knox et al., 2021), which could present another layer of complexity to the analysis. Future analyses could consider incorporating a broader range of sites spanning diverse vegetation types. This would ensure a more exhaustive assessment of parameter sensitivity across different ecosystems. Errors from external factors outside the methane biogeochemistry model, like heterotrophic respiration and net primary productivity, impact simulated methane emissions (Riley et al., 2011), which in turn affects the sensitivity analysis results. Despite these limitations, the findings from this study offer significant insights into the parametric sensitivity of various CH_4 emissions.

5. Conclusions

This study carried out a sensitivity analysis of 19 ELM model parameters with respect to methane emission from natural wetlands at 14 FLUXNET-CH_4 sites with diverse vegetation types. Machine learning-based emulators were employed to emulate the ELM model in consideration of computational demands. The GPR-based emulators were shown to represent the model simulations reasonably well across all the sites. These emulators were used to calculate the Sobol sensitivity indices for various CH_4 fluxes. Five parameters Q_{10} (CH_4 production), f_{D_0} (diffusion coefficient multiplier), f_{CH_4} (ratio between CH_4 and CO_2 production below the water table), z_τ (e-folding depth for decomposition), and K_{O_2} (O_2 half-saturation oxidation coefficient) were identified as sensitive parameters across various fluxes and sites. These five sensitive parameters accounted for approximately 95% of the total variance in emission. The remaining 14 parameters had negligible impact on emissions across all sites. Seasonal characteristics of parameter sensitivity to methane emissions showed specific features that long-term annual averages might overlook. The Comparison of the model simulations against FLUXNET-CH_4 observations revealed a potential for improving simulated emissions via parameter calibration. Future studies will focus on extending this sensitivity analysis to more FLUXNET-CH_4 sites to better understand how parametric sensitivities depend on vegetation types and climatic conditions. The identified sensitive parameters can be systematically adjusted to reduce the simulation error with respect to observed methane emissions using Bayesian calibration and ML-based emulators. In addition, the availability of high-quality observations from a diverse range of wetlands will greatly benefit this exercise.

Acknowledgments
The authors thank Earle A Killian III and Waidy Lee MIT Seed Fund for their generous financial support of this research. Q.Z. is supported by the Reducing Uncertainties in Biogeochemical Interactions through Synthesis and Computation (RUBISCO) Scientific Focus Area Project, sponsored by the Earth and Environmental Systems Modeling (EESM) Program under the Office of Biological and Environmental Research of the US Department of Energy Office of Science. The computations presented here were conducted using the "Svante" cluster, a facility located at MIT's Massachusetts Green High Performance Computing Center and jointly supported by the MIT Joint Program on the Science and Policy of Global Change; the Department of Earth, Atmospheric and Planetary Sciences; the Department of Civil and Environmental Engineering; the Institute for Data, Systems, and Society; and the Center for Global Change Science.

Data Availability Statement

The E3SM code is available at https://github.com/E3SM-Project/E3SM (Golaz et al., 2022). FLUXNET-CH_4 data is available for download at https://fluxnet.org/data/fluxnet-ch4-community-product/ (Delwiche et al., 2021; Knox et al., 2019). CRU JRA v2.2 data is available at https://catalogue.ceda.ac.uk/uuid/4bdf41fc10af4caaa489b14745c665a6 (Harris, 2021). The data and code are available at https://doi.org/10.5281/zenodo.12738074 (Chinta, 2024).

References

Arah, J. R. M., & Stephen, K. D. (1998). A model of the processes leading to methane emission from peatland. *Atmospheric Environment*, *32*(18), 3257–3264. https://doi.org/10.1016/s1352-2310(98)00052-1

Baki, H., Chinta, S., Balaji, C., & Srinivasan, B. (2022a). Determining the sensitive parameters of the weather research and forecasting (WRF) model for the simulation of tropical cyclones in the Bay of Bengal using global sensitivity analysis and machine learning. *Geoscientific Model Development*, *15*(5), 2133–2155. https://doi.org/10.5194/gmd-15-2133-2022

Baki, H., Chinta, S., Balaji, C., & Srinivasan, B. (2022b). Parameter calibration to improve the prediction of tropical cyclones over the Bay of Bengal using machine learning–based multiobjective optimization. *Journal of Applied Meteorology and Climatology*, *61*(7), 819–837. https://doi.org/10.1175/JAMC-D-21-0184.1

Balcombe, P., Speirs, J. F., Brandon, N. P., & Hawkes, A. D. (2018). Methane emissions: Choosing the right climate metric and time horizon. *Environmental Sciences: Processes and Impacts*, *20*(10), 1323–1339. https://doi.org/10.1039/c8em00414e

Bodelier, P. L. E., & Laanbroek, H. J. (2004). Nitrogen as a regulatory factor of methane oxidation in soils and sediments. *FEMS Microbiology Ecology*, *47*(3), 265–277. https://doi.org/10.1016/s0168-6496(03)00304-0

Bousquet, P., Ciais, P., Miller, J. B., Dlugokencky, E. J., Hauglustaine, D. A., Prigent, C., et al. (2006). Contribution of anthropogenic and natural sources to atmospheric methane variability. *Nature*, *443*(7110), 439–443. https://doi.org/10.1038/nature05132

Bridgham, S. D., Cadillo-Quiroz, H., Keller, J. K., & Zhuang, Q. (2013). Methane emissions from wetlands: Biogeochemical, microbial, and modeling perspectives from local to global scales. *Global Change Biology*, *19*(5), 1325–1346. https://doi.org/10.1111/gcb.12131

Bridgham, S. D., Megonigal, J. P., Keller, J. K., Bliss, N. B., & Trettin, C. (2006). The carbon balance of North American wetlands. *Wetlands*, *26*(4), 889–916. https://doi.org/10.1672/0277-5212(2006)26[889:tcbona]2.0.co;2

Chinta, S. (2024). Dataset for "machine learning driven sensitivity analysis of E3SM land model parameters for wetland methane emissions [Dataset]. *Zenodo*. https://doi.org/10.5281/zenodo.12738074

Chinta, S., & Balaji, C. (2020). Calibration of WRF model parameters using multiobjective adaptive surrogate model-based optimization to improve the prediction of the Indian summer monsoon. *Climate Dynamics*, *55*(3–4), 631–650. https://doi.org/10.1007/s00382-020-05288-1

Chinta, S., Gao, X., & Zhu, Q. (2023). Machine learning assisted Bayesian calibration of model physics parameters for wetland methane emissions: A case study at a FLUXNET-CH4 site. *NeurIPS 2023 Workshop on Tackling Climate Change with Machine Learning*. https://www.climatechange.ai/papers/neurips2023/79

Chinta, S., Yaswanth Sai, J., & Balaji, C. (2021). Assessment of WRF model parameter sensitivity for high-intensity precipitation events during the Indian summer monsoon. *Earth and Space Science*, *8*(6), e2020EA001471. https://doi.org/10.1029/2020ea001471

Ciais, P., Sabine, C., Bala, G., Bopp, L., Brovkin, V., Canadell, J., et al. (2013). Carbon and other biogeochemical cycles. In *Climate change 2013: The physical science basis. Contribution of working group I to the fifth assessment report of the intergovernmental panel on climate change* (pp. 465–570). Cambridge University Press.

Dagon, K., Sanderson, B. M., Fisher, R. A., & Lawrence, D. M. (2020). A machine learning approach to emulation and biophysical parameter estimation with the Community Land Model, version 5. *Advances in Statistical Climatology, Meteorology and Oceanography*, *6*(2), 223–244. https://doi.org/10.5194/ascmo-6-223-2020

Delwiche, K. B., Knox, S. H., Malhotra, A., Fluet-Chouinard, E., McNicol, G., Feron, S., et al. (2021). FLUXNET-CH_4: A global, multi-ecosystem dataset and analysis of methane seasonality from freshwater wetlands. *Earth System Science Data*, *13*(7), 3607–3689. https://doi.org/10.5194/essd-13-3607-2021

Dlugokencky, E. J., Bruhwiler, L., White, J. W. C., Emmons, L. K., Novelli, P. C., Montzka, S. A., et al. (2009). Observational constraints on recent increases in the atmospheric CH_4 burden. *Geophysical Research Letters*, *36*(18). https://doi.org/10.1029/2009gl039780

Etminan, M., Myhre, G., Highwood, E. J., & Shine, K. P. (2016). Radiative forcing of carbon dioxide, methane, and nitrous oxide: A significant revision of the methane radiative forcing. *Geophysical Research Letters*, *43*(24), 12612–614623. https://doi.org/10.1002/2016gl071930

Fisher, R. A., Wieder, W. R., Sanderson, B. M., Koven, C. D., Oleson, K. W., Xu, C., et al. (2019). Parametric controls on vegetation responses to biogeochemical forcing in the CLM5. *Journal of Advances in Modeling Earth Systems*, *11*(9), 2879–2895. https://doi.org/10.1029/2019ms001609

Gao, X., Avramov, A., Saikawa, E., & Adam Schlosser, C. (2021). Emulation of community land model version 5 (Clm5) to quantify sensitivity of soil moisture to uncertain parameters. *Journal of Hydrometeorology*, *22*(2), 259–278. https://doi.org/10.1175/JHM-D-20-0043.1

Gattiker, J., Myers, K., Williams, B., Higdon, D., Carzolio, M., & Hoegh, A. (2016). Gaussian process-based sensitivity analysis and Bayesian model calibration with GPMSA. In R. Ghanem, D. Higdon, & H. Owhadi (Eds.), *Handbook of uncertainty quantification* (pp. 1–41). Springer International Publishing. https://doi.org/10.1007/978-3-319-11259-6_58-1

Golaz, J.-C., Caldwell, P. M., Van Roekel, L. P., Petersen, M. R., Tang, Q., Wolfe, J. D., et al. (2019). The DOE E3SM coupled model version 1: Overview and evaluation at standard resolution. *Journal of Advances in Modeling Earth Systems*, *11*(7), 2089–2129. https://doi.org/10.1029/2018ms001603

Golaz, J.-C., Van Roekel, L. P., Zheng, X., Roberts, A. F., Wolfe, J. D., Lin, W., et al. (2022). The DOE E3SM Model Version 2: Overview of the physical model and initial model evaluation. *Journal of Advances in Modeling Earth Systems*, *14*(12). https://doi.org/10.1029/2022ms003156

Gong, W., Duan, Q., Li, J., Wang, C., Di, Z., Dai, Y., et al. (2015). Multi-objective parameter optimization of common land model using adaptive surrogate modeling. *Hydrology and Earth System Sciences*, *19*(5), 2409–2425. https://doi.org/10.5194/hess-19-2409-2015

Gurevitch, J., & Mengersen, K. (2019). *Handbook of meta-analysis in ecology and evolution*. Princeton University Press.

Gurney, K. (2018). *An introduction to neural networks*. CRC press.

Gutmann, H.-M. (2001). A radial basis function method for global optimization. *Journal of Global Optimization*, *19*(3), 201–227. https://doi.org/10.1023/a:1011255519438

Harris, I. C. (2021). CRU JRA v2.2: A forcings dataset of gridded land surface blend of climatic research unit (CRU) and Japanese reanalysis (JRA) data; Jan.1901 - Dec.2020. https://catalogue.ceda.ac.uk/uuid/4bdf41fc10af4caaa489b14745c665a6

Iman, R. L., Helton, J. C., & Campbell, J. E. (1981). An approach to sensitivity analysis of computer models: Part I—Introduction, input variable selection and preliminary variable assessment. *Journal of Quality Technology*, *13*(3), 174–183. https://doi.org/10.1080/00224065.1981.11978748

IPCC. (2013). Climate change 2013: The physical science basis. *Contribution of Working Group I to the Fifth Assessment Report of the Intergovernmental Panel on Climate Change*.

Jackson, R. B., Saunois, M., Bousquet, P., Canadell, J. G., Poulter, B., Stavert, A. R., et al. (2020). Increasing anthropogenic methane emissions arise equally from agricultural and fossil fuel sources. *Environmental Research Letters*, *15*(7), 71002. https://doi.org/10.1088/1748-9326/ab9ed2

Kennedy, M. C., & O'Hagan, A. (2001). Bayesian calibration of computer models. *Journal of the Royal Statistical Society: Series B*, *63*(3), 425–464. https://doi.org/10.1111/1467-9868.00294

Kirschke, S., Bousquet, P., Ciais, P., Saunois, M., Canadell, J. G., Dlugokencky, E. J., et al. (2013). Three decades of global methane sources and sinks. *Nature Geoscience*, *6*(10), 813–823. https://doi.org/10.1038/ngeo1955

Knox, S. H., Bansal, S., McNicol, G., Schafer, K., Sturtevant, C., Ueyama, M., et al. (2021). Identifying dominant environmental predictors of freshwater wetland methane fluxes across diurnal to seasonal time scales. *Global Change Biology*, *27*(15), 3582–3604. https://doi.org/10.1111/gcb.15661

Knox, S. H., Jackson, R. B., Poulter, B., McNicol, G., Fluet-Chouinard, E., Zhang, Z., et al. (2019). FLUXNET-CH4 synthesis activity: Objectives, observations, and future directions. *Bulletin of the American Meteorological Society*, *100*(12), 2607–2632. https://doi.org/10.1175/BAMS-D-18-0268.1

Koven, C. D., Riley, W. J., Subin, Z. M., Tang, J. Y., Torn, M. S., Collins, W. D., et al. (2013). The effect of vertically resolved soil biogeochemistry and alternate soil C and N models on C dynamics of CLM4. *Biogeosciences*, *10*(11), 7109–7131. https://doi.org/10.5194/bg-10-7109-2013

Lan, X., Thoning, K. W., & Dlugokencky, E. J. (2023). Trends in globally-averaged CH_4, N_2O, and SF_6 determined from NOAA global monitoring laboratory measurements.

Loeppky, J. L., Sacks, J., & Welch, W. J. (2009). Choosing the sample size of a computer experiment: A practical guide. *Technometrics*, *51*(4), 366–376. https://doi.org/10.1198/tech.2009.08040

McKay, M. D., Conover, W. J., & Beckman, R. J. (1979). A comparison of three methods for selecting values of input variables in the analysis of output from a computer code. *Technometrics*, *21*(2), 239–245. https://doi.org/10.1080/00401706.1979.10489755

Melton, J. R., Wania, R., Hodson, E. L., Poulter, B., Ringeval, B., Spahni, R., et al. (2013). Present state of global wetland extent and wetland methane modelling: Conclusions from a model intercomparison project (WETCHIMP). *Biogeosciences*, *10*(11), 753–788. https://doi.org/10.5194/bg-10-753-2013

Müller, J., Paudel, R., Shoemaker, C. A., Woodbury, J., Wang, Y., & Mahowald, N. (2015). CH4 parameter estimation in CLM4.5bgc using surrogate global optimization. *Geoscientific Model Development*, *8*(10), 3285–3310. https://doi.org/10.5194/gmd-8-3285-2015

Nisbet, E. G., Manning, M. R., Dlugokencky, E. J., Fisher, R. E., Lowry, D., Michel, S. E., et al. (2019). Very strong atmospheric methane growth in the 4 years 2014–2017: Implications for the Paris Agreement. *Global Biogeochemical Cycles*, *33*(3), 318–342. https://doi.org/10.1029/2018gb006009

Oleson, K. W., Lawrence, D. M., Bonan, G. B., Drewniak, B., Huang, M., Koven, C. D., et al. (2013). Technical description of version 4.5 of the community land model (CLM). NCAR Technical Note, NCAR/TN-503+STR.

Papa, F., Prigent, C., Aires, F., Jimenez, C., Rossow, W. B., & Matthews, E. (2013). Interannual variability of surface water extent at the global scale, 1993–2004. *Journal of Geophysical Research: Atmospheres*, *115*(D12). https://doi.org/10.1029/2009jd012674

Poulter, B., Bousquet, P., Canadell, J. G., Ciais, P., Peregon, A., Saunois, M., et al. (2017). Global wetland contribution to 2000–2012 atmospheric methane growth rate dynamics. *Environmental Research Letters*, *12*(9), 94013. https://doi.org/10.1088/1748-9326/aa8391

Rasmussen, C. E., & Williams, C. K. I. (2006). *Gaussian processes for machine learning*. MIT Press.

Reddy, P. J., Chinta, S., Matear, R., Taylor, J., Baki, H., Thatcher, M., et al. (2023). Machine learning based parameter sensitivity of regional climate models—A case study of the WRF model for heat extremes over Southeast Australia. *Environmental Research Letters*, *19*(1), 14010. https://doi.org/10.1088/1748-9326/ad0eb0

Ricciuto, D., Sargsyan, K., & Thornton, P. (2018). The impact of parametric uncertainties on biogeochemistry in the E3SM land model. *Journal of Advances in Modeling Earth Systems*, *10*(2), 297–319. https://doi.org/10.1002/2017ms000962

Ricciuto, D. M., Xu, X., Shi, X., Wang, Y., Song, X., Schadt, C. W., et al. (2021). An integrative model for soil biogeochemistry and methane processes: I. Model structure and sensitivity analysis. *Journal of Geophysical Research: Biogeosciences*, *126*(8), e2019JG005468. https://doi.org/10.1029/2019jg005468

Riley, W. J., Subin, Z. M., Lawrence, D. M., Swenson, S. C., Torn, M. S., Meng, L., et al. (2011). Barriers to predicting changes in global terrestrial methane fluxes: Analyses using CLM4Me, a methane biogeochemistry model integrated in CESM. *Biogeosciences*, *8*(7), 1925–1953. https://doi.org/10.5194/bg-8-1925-2011

Rosentreter, J. A., Borges, A. V., Deemer, B. R., Holgerson, M. A., Liu, S., Song, C., et al. (2021). Half of global methane emissions come from highly variable aquatic ecosystem sources. *Nature Geoscience*, *14*(4), 225–230. https://doi.org/10.1038/s41561-021-00715-2

Sakabe, A., Takahashi, K., Azuma, W., Itoh, M., Tateishi, M., & Kosugi, Y. (2021). Controlling factors of seasonal variation of stem methane emissions from Alnus japonica in a riparian wetland of a temperate forest. *Journal of Geophysical Research: Biogeosciences*, *126*(10), e2021JG006326. https://doi.org/10.1029/2021jg006326

Saltelli, A., Ratto, M., Andres, T., Campolongo, F., Cariboni, J., Gatelli, D., et al. (2008). *Global sensitivity analysis: The primer*. John Wiley and Sons.

Saunois, M., Bousquet, P., Poulter, B., Peregon, A., Ciais, P., Canadell, J. G., et al. (2016). The global methane budget 2000-2012. *Earth System Science Data*, *8*(2), 697–751. https://doi.org/10.5194/essd-8-697-2016

Shindell, D., Kuylenstierna, J. C. I., Vignati, E., van Dingenen, R., Amann, M., Klimont, Z., et al. (2012). Simultaneously mitigating near-term climate change and improving human health and food security. *Science*, *335*(6065), 183–189. https://doi.org/10.1126/science.1210026

Sobol, I. M. (2001). Global sensitivity indices for nonlinear mathematical models and their Monte Carlo estimates. *Mathematics and Computers in Simulation*, *55*(1–3), 271–280. https://doi.org/10.1016/s0378-4754(00)00270-6

Song, C., Luan, J., Xu, X., Ma, M., Aurela, M., Lohila, A., et al. (2020a). A microbial functional group-based CH_4 model integrated into a terrestrial ecosystem model: Model structure, site-level evaluation, and sensitivity analysis. *Journal of Advances in Modeling Earth Systems*, *12*(4). https://doi.org/10.1029/2019MS001867

Song, C., Luan, J., Xu, X., Ma, M., Aurela, M., Lohila, A., et al. (2020b). A microbial functional group-based CH_4 model integrated into a terrestrial ecosystem model: Model structure, site-level evaluation, and sensitivity analysis. *Journal of Advances in Modeling Earth Systems*, *12*(4), e2019MS001867. https://doi.org/10.1029/2019ms001867

Turetsky, M. R., Kotowska, A., Bubier, J., Dise, N. B., Crill, P., Hornibrook, E. R. C., et al. (2014). A synthesis of methane emissions from 71 northern, temperate, and subtropical wetlands. *Global Change Biology*, *20*(7), 2183–2197. https://doi.org/10.1111/gcb.12580

Wang, C., Duan, Q., Gong, W., Ye, A., Di, Z., & Miao, C. (2014). An evaluation of adaptive surrogate modeling based optimization with two benchmark problems. *Environmental Modelling and Software*, *60*, 167–179. https://doi.org/10.1016/j.envsoft.2014.05.026

Wang, C., Qian, Y., Duan, Q., Huang, M., Berg, L. K., Shin, H. H., et al. (2020a). Assessing the sensitivity of land-atmosphere coupling strength to boundary and surface layer parameters in the WRF model over Amazon. *Atmospheric Research*, *234*, 104738. https://doi.org/10.1016/j.atmosres.2019.104738

Wang, H., Gong, W., Duan, Q., & Di, Z. (2020b). Evaluation of parameter interaction effect of hydrological models using the sparse polynomial chaos (SPC) method. *Environmental Modelling and Software*, *125*, 104612. https://doi.org/10.1016/j.envsoft.2019.104612

Wang, J. (2020). An intuitive tutorial to Gaussian processes regression. *ArXiv Preprint ArXiv:2009.10862*.

Xu, X., Elias, D. A., Graham, D. E., Phelps, T. J., Carroll, S. L., Wullschleger, S. D., & Thornton, P. E. (2012). A microbial functional group-based module for simulating methane production and consumption: Application to an incubated permafrost soil. *Journal of Geophysical Research*, *117*(G3).

Yuan, F., Wang, Y., Ricciuto, D. M., Shi, X., Yuan, F., Hanson, P. J., et al. (2021). An integrative model for soil biogeochemistry and methane processes. II: Warming and elevated CO_2 effects on peatland CH_4 emissions. *Journal of Geophysical Research: Biogeosciences*, *126*(8), e2020JG005963. https://doi.org/10.1029/2020JG005963

Zhang, S., Zhang, F., Shi, Z., Qin, A., Wang, H., Sun, Z., et al. (2020). Sources of seasonal wetland methane emissions in permafrost regions of the Qinghai-Tibet Plateau. *Scientific Reports*, *10*(1), 7520. https://doi.org/10.1038/s41598-020-63054-z

Zhu, Q., Liu, J., Peng, C., Chen, H., Fang, X., Jiang, H., et al. (2014). Modelling methane emissions from natural wetlands by development and application of the TRIPLEX-GHG model. *Geoscientific Model Development*, *7*(3), 981–999. https://doi.org/10.5194/gmd-7-981-2014

Zhu, Q., Riley, W. J., Tang, J., Collier, N., Hoffman, F. M., Yang, X., & Bisht, G. (2019). Representing nitrogen, phosphorus, and carbon interactions in the E3SM land model: Development and global benchmarking. *Journal of Advances in Modeling Earth Systems*, *11*(7), 2238–2258. https://doi.org/10.1029/2018ms001571